THE PENNSYLVANIA STATE UNIVERSITY
SCHREYER HONORS COLLEGE

DEPARTMENT OF BIOLOGY

The Role of Cytoplasmic Domain Contacts in the Functional Relationship Between the Voltage Sensor and Pore of Elk Family Potassium Channels

EVAN MANCINI
SPRING 2024

A thesis
submitted in partial fulfillment
of the requirements
for a baccalaureate degree
in Biology
with honors in Biology

Reviewed and approved* by the following:

Timothy Jegla
Associate Professor of Biology, Associate Department Head of Graduate Education
Thesis Supervisor

Sarah M. Assmann
Wallar Professor of Biology
Honors Adviser

* Electronic approvals are on file.

ABSTRACT

Voltage-gated ion channels are a broad class of proteins commonly found in neurons. These proteins can be activated by either hyperpolarized or depolarized membrane potentials and regulate resting membrane potential, membrane resistance, and action potential generation and frequency. This electric current allows neurons to communicate and is the fundamental mechanism of signaling within the nervous system (Kandel et al., 2013). This research investigates the voltage-gated potassium channel human Elk1. The Elk1 subfamily falls within the Ether-a-go-go (EAG) gene family, a group of channels in the CNBD superfamily that are expressed and cardiovascular systems (Codding et al., 2020). The outward potassium current of these channels produces the refractory phase of the action potential. hElk1 channels are comprised of a functionally independent voltage sensor and pore that interact during depolarized membrane potentials to conduct an ion current (Engeland et al., 1998). Past studies have found that when the peptide linkage between these structures (S4-S5 Linker) is severed in other EAG family channels, the channels retain their function with only a minor shift in conductivity. This suggests the presence of other non-covalent interactions that further stabilize the channel (Lorinczi et al., 2015). This research investigates whether physical contact with the N-terminal cytoplasmic Per-Arnt-Sim (PAS) domain attached to the VSD is important for functional association of the VSD and PD in split channels. We attained novel results that hElk1 was still functional when lacking an intact S4-S5 linker and showed only a delay in activation to more depolarized voltages. Consistent with past studies, we also found that hElk1 was able to function with a truncated PAS domain (Li et al., 2015). The severance of the full PAS domain and S4-S5 linker together rendered hElk1 channels nonfunctional, while the severance of only the PAS-cap and the S4-S5 linker expressed a transient inactivating current. We also observed that split channels lacking the PAS domain still trafficked to the membrane, meaning the lack of current in these channels is due to a gating issue. These findings suggest that the PAS domain and S4-S5 linker both contribute to the open state stability of hElk1. However, the exact method of interaction between these

structures must be further elucidated. Future research should further elucidate the method of this interaction and investigate interactions between split channels and phospholipid contacts in the cell membrane, specifically PIP_2.

TABLE OF CONTENTS

LIST OF FIGURES

ACKNOWLEDGEMENTS

I would like to thank Dr. Jegla for allowing me to work in his laboratory since the beginning of my sophomore year. I know how difficult it can be to bring in a new student who has no wet lab experience. His knowledge of our areas of interest and his guidance on my projects has helped me grow tremendously throughout my undergraduate research career.

Thank you to my Honors Advisor, Dr. Assmann. Her great wisdom helped me not only progress through my thesis, but also plan my classes each semester, my summer engagements, and most notably, my application to medical school. She was always someone I knew I could talk to when I was faced with a difficult dilemma.

I would also like to thank graduate student Ben Simonson, my mentor in the lab daily. Especially in my first year, I relied on him extremely heavily to direct me in my everyday tasks as I was learning how to perform research. He was extremely patient even when I would ask him hundreds of questions a day or run an experiment incorrectly. He explained complex electrophysiological topics and methods in a way that I was able to easily comprehend, even with no prior understanding.

I also deeply appreciate the Schreyer Honors College for not only providing me with this opportunity to lead my own undergraduate research, but for funding my research while I worked in my laboratory during the summer of 2022.

Lastly, I would like to share my gratitude for my family, friends, and classmates for providing me with unwavering support even in difficult times when I doubted my own capabilities. Without them I would not be who I am today.

Chapter 1: Introduction

Ion Channels

Ion channels are a broad class of proteins that support a wide variety of functions in cells of the human nervous system. They are integral surface proteins embedded in the plasma membrane that conduct an electrical current into or out of the cell. This current results from the flow of ions through the pore of the channel. Most ion channels are selective toward one type of ion, the most common being potassium (K^+), sodium (Na^+), chlorine (Cl^-), and calcium (Ca^{2+}). The charge of these ions, combined with their electrochemical gradient and the membrane potential of the cell, dictate the direction of current flow and the overall change of the cell's charge. Under a specific stimulus, the protein changes its conformation from a "closed" to an "open" state, allowing ions to pass through (Kandel et al., 2013).

Different families of ion channels are activated by different stimuli, a common one being changes in the membrane electric field. These channels, deemed "voltage-gated ion channels," are responsible for regulating the resting membrane potential and membrane resistance, as well as generating the action potential.

Human Ether-Á-Go-Go-Like-Potassium (hElk) Channels

The *ether-á-go-go* (EAG) superfamily is one of the many classes of voltage-gated potassium ion channels and are responsible for various aspects of the electric activity of the cell. The subfamily consists of Eag (Kv10), hErg (human EAG-related gene / Kv11), and hElk (human EAG-like K^+ / Kv12) (Warmke and Ganetzky, 1994). The channels are distributed in various regions of the nervous and cardiovascular system: hEag channels are found throughout the central nervous system, hErg channels are

found in the myocardial myocytes, and hElk channels are found in the hippocampus, suprachiasmatic nucleus, and cortical brain regions (Saganich et al., 1999) (Zou et al., 2003) (Curran et al., 1995) (Hermanstyne et al., 2023). These channels are responsible for various aspects of a cell's electrical signaling. Eag channels are suggested to regulate action potential frequency from presynaptic terminals (Mortensen et al., 2015). Erg channels have been found to mediate the refractory period of action potentials in the heart (Mitcheson et al., 2000). Contrarily, Elk channels have been found to regulate subthreshold hyperpolarizing potassium currents (Zhang et al., 2010).

Though their location may differ, the tertiary structure of these channels is highly conserved. EAG superfamily channels are composed of four subunits, which can be either closely related (heteromeric) or identical (homomeric) (Jones et al., 2004). Each subunit consists of an N-terminal Per-Arnt-Sim (PAS) domain and a C-terminal Cyclic Nucleotide-Binding Homology domain (CNBHD). There are six transmembrane domains in each subunit: S2 through S4 make up the voltage sensor domain (VSD), whereas S5 and S6 make up the pore domain (PD) (Figure 1). The subunits are organized so that the four sets of S5 and S6 units are positioned internally to create the pore of the channel. Contrarily, the four VSDs do not interact with one another because they sit outside of the pore. Connecting the VSD and the PD is a short amino-acid sequence known as the S4-S5 Linker (Figure 1). This structure is responsible for translating the change in VSD conformation to the conformation of the pore in states of depolarization and repolarization (Jogini and Roux, 2005) (Labro et al., 2008).

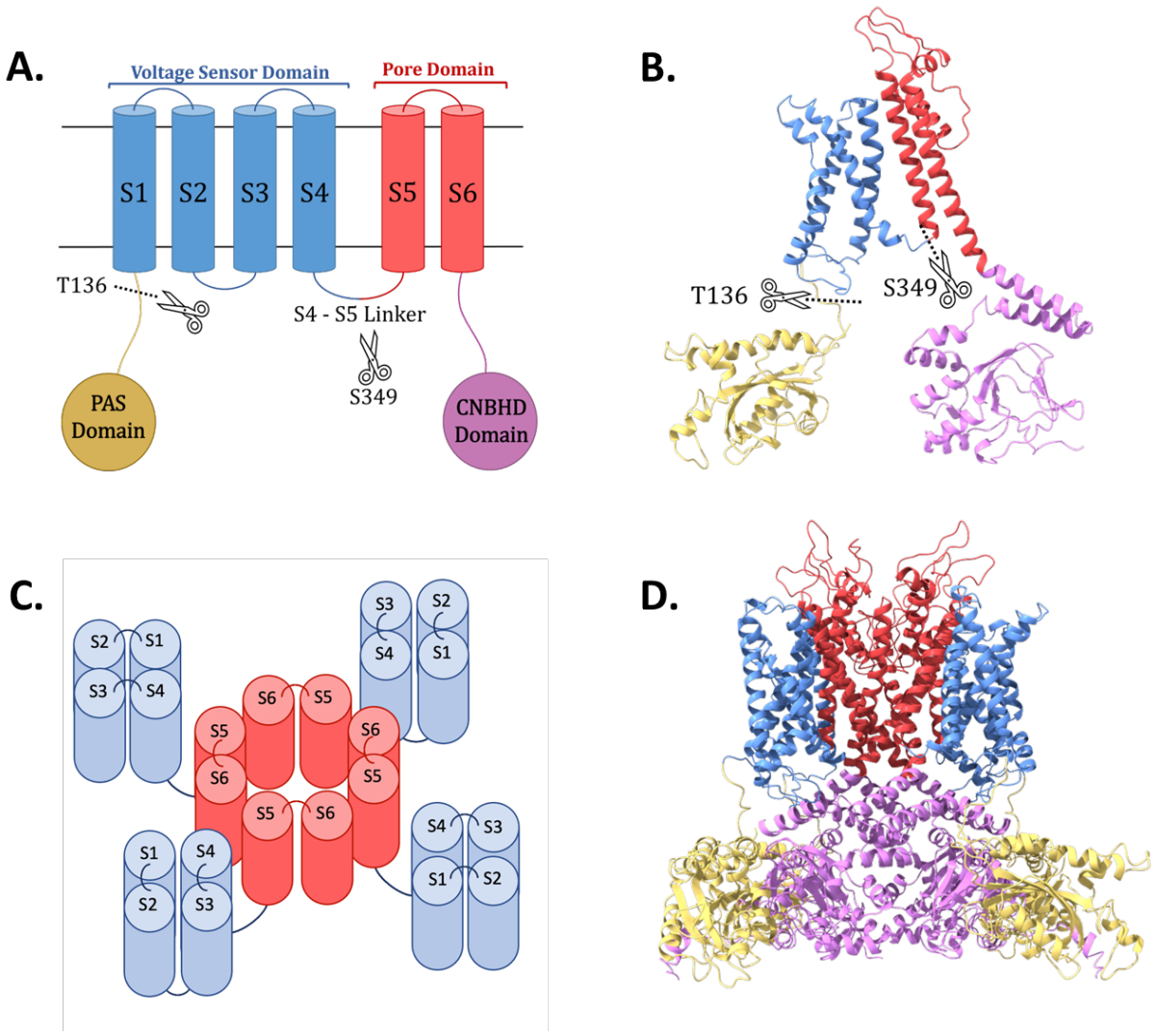

Figure 1: Structure of hElk monomer and tetramer

(A) Schematic representation of a single hElk subunit and the sites where covalent links were severed in experiments. (B) Tertiary structure of a single hElk subunit with cut sites identified. (C) Schematic representation of the homotetrameric hElk structure. The pore domains are red, and the voltage sensors are blue. (D) Homotetrameric tertiary structure of hElk, composed of four subunits. The colors represent the same regions as the colors in A and B.

Domain Swapping

Potassium channel families like Kv1.2 experience domain swapping (Codding et al., 2020). Domain swapping occurs when the VSD and PD are distanced by a longer S4-S5 linker. To retain a compact shape, the VSD of a subunit is positioned closer to the PD of the neighboring subunit than its own. Therefore, the linker connecting the VSD to its corresponding PD is positioned under the S6 transmembrane domain of the neighboring PD. This has led to the hypothesis that the S4-S5 linker can directly control the state of the pore via interactions with the S6 transmembrane domain of the neighboring PD (Jensen et al., 2018).

On the other hand, the EAG superfamily does not exhibit domain swapping because of the shortened length of the S4-S5 linker (Wang & MacKinnon, 2017). This means that the VSD sits directly behind its corresponding PD. Because this linker does not pass under the S6 transmembrane domain and pore of the channel, it is believed to function in an alternate way to modulate the opening and closing of the channel (Whicher and MacKinnon, 2016).

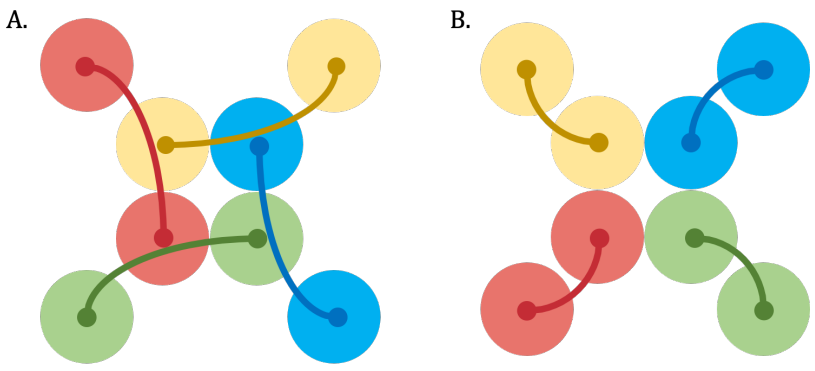

Figure 2: Domain swapped and non-domain swapped channel.

(A) Representation of a domain-swapped homotetrameric channel. (B) Representation of a non-domain swapped homotetrameric channel. The color of each PD (inner units) and VSD (outer units) represent a monomer of the channel. Lines connecting the PDs and VSDs represent the S4-S5 linker.

Potassium Channel Gating Mechanics and the S4-S5 Linker

The exact mechanism by which gating occurs in voltage-gated potassium channels is not fully understood. Recent evidence suggests that different families of voltage-gated potassium channels exhibit different gating mechanics, likely due to the presence or absence of domain swapping (Codding et al., 2020) (Whicher & MacKinnon, 2016). In domain swapped Kv1.2 channels, depolarization forces the S4 transmembrane domain toward the extracellular space. The altered electric field influences the charged residues within the S4 domain to shift to form salt bridges with negative residues inside the VSD (Jensen et al., 2012). The movement of the S4 transmembrane domain tightens the S4-S5 linker, which changes its interaction with the bottom of the S6 transmembrane domain to open the pore (Ruta et al., 2005) (Durell & Guy, 1992). Once the membrane potential repolarizes, the S4 transmembrane domain shifts back downward, which loosens the S4-S5 linker and reestablishes the 'closed' conformation of the S5 and S6 transmembrane domains (Jogini and Roux, 2005) (Durell & Guy, 1992) (Ruta et al., 2005). Thus, the S4-S5 linker serves to translate the mechanical movement of the VSD to the PD to open and close the Kv1.2 channel (Jensen et al., 2012) (Long et al., 2005).

The lack of a direct connection between the S4-S5 linker and the bottom of the S6 transmembrane domain in EAG channels suggests the mechanism of gating may rely on other factors, but the exact mechanism is still not well-understood (Whicher and MacKinnon, 2016) (Zhang et al., 2009). If the EAG superfamily S4-S5 linker performed the same mechanical translation process that it did in Kv1.2 and other domain-swapped channels, then severing the linker would prevent the pore from opening at any voltage. However, studies have found that the severance of the S4-S5 linker does not eliminate gating, but rather delays the channel's activation toward higher voltages (Figure 1A, 1B) (de la Peña et al., 2017) (Li et al., 2015) (Tomczak et al., 2017). These findings suggest that the S4-S5 linker functions differently in EAG channels and may experience steric interactions with other parts of the channel.

Even the channels within the EAG superfamily vary in their gating dynamics. There are three major types of conformations that voltage-gated channels can assume. As standard delayed-rectifying channels, Eag1 and Elk1 channels alternate between two of these conformations: an open state, during depolarized potentials, and a closed-deactivated state, during hyperpolarized potentials (Engeland et al., 1998) (Robertson et al., 1996). Other channels, like hErg1, experience a second closed state due to inactivation (Trudeau et al., 1995). The closed-deactivated state occurs when the channel closes due to a hyperpolarizing potential, and these channels can achieve the open conformation from this closed state. Conversely, the closed-inactivated state occurs during a depolarized potential when the channel becomes unstable and switches to a closed state that is more energetically and sterically favorable. Although channels can recover from the inactivated state to the open state, this process is very slow at depolarized voltages. Thus, recovery from the inactivated state must often occur at hyperpolarized or resting membrane potential. As a result, experiments testing inactivating channels will often issue a hyperpolarizing voltage that forces closed-inactivated channels back to the closed-deactivated conformation to allow them to reopen.

The PAS Domain

Another area of interest within the structure of EAG channels is the PAS domain. This structure, comprising the first 130 amino acids, represents the N-terminal cytoplasmic domain. It is made up of mostly β-sheets flanked by a surrounding α-helices to form a ball-shaped structure (Figure 3). Within the PAS domain is a specified area known as the PAS-cap that constitutes the first 25 amino acids of the channel, consisting of both an unstructured region and an amphipathic α-helix (Ng et al., 2011) (Morais Cabral et al., 1998). Although the extent of the PAS domain's function is not fully known, it is well-established that it plays an important regulatory role in channel gating. The presence of a hydrophobic binding pocket within the domain in Eag channels has been shown to bind drug ligands. Both imipramine

and chlorpromazine were shown to have an inhibitory effect on channel current, as they shifted the activation of the channel to more depolarized voltages and lowered the peak current expressed, respectively (Wang et al., 2020) (Wang et al., 2023). The domain has also been shown to play a critical role in open-state stabilization, as its deletion confers a much faster rate of deactivation in Erg channels (Li et al., 2015). Mutations in this region in Erg channels have been shown to cause a cardiac disorder known as Long-QT syndrome, further emphasizing the importance of this domain (Chen et al., 1999).

It is well-established that the PAS domain interacts with the CNBHD domain of EAG channels throughout the gating process, but many of these residues are past the PAS-cap (Haitin et al., 2013) (Li et al., 2014) (Gustina & Trudeau, 2012). The PAS domain has been shown to play an important role in the open-state stabilization of hElk1 channels, as its deletion delays the voltage-dependent conductivity of the channel (Li et al., 2015). In addition to the PAS domain's interactions with the CNBHD domain, residues in both the PAS domain and the PAS-cap are also suggested to interact with the S4-S5 linker. NMR titration experiments demonstrated that a peptide mimicking the S4-S5 linker experienced significant interactions with multiple residues in the PAS domain (Li et al., 2010). Furthermore, Erg channels with a removed PAS-cap exhibit a faster deactivation than their WT counterparts (Ng et al., 2011). When S4-S5 linker residues of WT Erg channels were mutated, their kinetics showed a phenotype similar to those with the PAS-cap removed. This suggests that these mutated residues in the S4-S5 linker interfered with an interaction between the PAS-cap and the linker (Wang et al., 1998). The presence of a recombinant PAS-cap has also been shown to restore the WT gating phenotype in Erg channels with the PAS-cap removed (Wang et al., 2000) (Gustina & Trudeau, 2009).

The interaction between the PAS domain and S4-S5 linker, as well as their hypothesized involvement in gating, make them an intriguing area for investigation in hElk1. With hElk1 being an understudied channel despite its dispersion throughout the nervous system, these results may elucidate a unique mechanism of gating and determine which aspects of this process are conserved among the EAG gene family.

Chapter 2: Methods

Molecular Biology

The human Elk1 (Kv12.1, KCNH8) gene was derived from whole-brain RNA using PCR techniques and inserted into the pOX-ER plasmid (Zhang et al., 2009). This wild-type channel clone matches the amino acid sequence of the hElk1 protein registered in GenBank as NM 144633.

Cloning techniques were derived from those outlined in Kazmierczak et al., 2013. The S349 split, D2-23, and D2-136 + S349 split constructs were amplified from WT hElk1 in pOX-ER plasmid via oligo-mediated PCR mutagenesis. The D2-136 hElk1 mutant, first characterized by Li et al., 2015, was also amplified in this manner. The primers for these reactions were designed to include restriction enzyme cut sites and the Kozak sequence. PCR products and WT pOX-ER were digested with the same restriction enzymes and then ligated using T4 DNA Ligase (New England Biolabs, Ipswich, MA) to create a plasmid construct.

The D2-23 + S349 split and the independent PAS domain mutants were amplified from WT hElk1 in a novel way, using primers with annealing sites outside of the target construct. Resulting PCR products thus contained not only the target construct, but also the T3 promoter, 3' untranslated region, and 5' untranslated region of the pOX plasmid. With the inclusion of these regions in the PCR product, the construct could be directly transcribed into RNA without restriction enzyme digests, ligations, or competent cell transformations.

To tag the PD of hElk1 with GFP, overlap PCR was used. Each component was first amplified independently – the PD from WT hElk1, and the GFP from an eGFP construct in pOX-ER. The primers for these PCR reactions were formulated to include an overhang region that would not anneal with the single stranded DNA. This would serve as a nucleotide bridge that could connect the pore domain and GFP PCR constructs. This was done by adding an 18-nucleotide sequence to the end of the reverse primer in the pore domain reaction and at the start of the forward primer in the GFP reaction. Both amplified

constructs were combined in the same PCR reaction, where this overlapping nucleotide sequence allowed them to anneal to one-another and create a GFP-tagged hElk1 pore domain construct. The amino acid code for this sequence was Gly-Gly-Ser-Gly-Gly-Ser. The nucleotide bridge was an abbreviated version of the one used by Tomczak and colleagues, who found this bridge to have no interference with the properties of the channel given the nonpolar characteristics of these amino acids (Tomczak et al., 2017).

All PCR products were purified in water using QIAprep Spin Miniprep Kits (Qiagen, Germantown, MD). Constructs were verified using third-party Sanger sequencing (Azenta, South Plainfield, NJ) and whole-plasmid sequencing (Plasmidosaurus, Louisville, KY).

The recombinant plasmid products and the PCR products containing transcription sites were linearized using the Not-1 enzyme and then underwent capped cRNA synthesis via the T3 mMessge mMachine kit (Life Technologies). Samples were purified using LiCl precipitation and washed in cold 70% ethanol. The dried pellet of RNA product was redissolved in a 20:1 dilution of nuclease-free water and SUPERase-In (Life Technologies), an RNAse inhibitor enzyme.

Xenopus laevis Oocyte Injections

Xenopus ovaries were supplied by Xenopus 1 (Ann Arbor, MI). Methods of processing oocytes was adapted from Pisupati et al., 2018. The ovaries were manually broken apart with tweezers before digesting in 75mL of 1mg/ml Type II collagenase (Sigma Aldrich, St Louis, MO) in Ca^{2+}-free ND98solution (98mM NaCl, 2mM KCl, 1mM $MgCl_2$, and 5mM HEPES, pH 7.2) on a rotatory shaker. If defolliculation of the ovary membrane was incomplete after 1 hour, oocytes were rinsed in Ca^{2+}- free solution and digested a second time for 20 minutes. High-quality, mature oocytes were manually sorted from the digested ovaries and suspended in ND98 Culture solution (98mM NaOH, 2mM KCl, 1.8mM $CaCl_2$, 1mM $MgCl_2$, 5mM HEPES, 2.5mM Na-Pyruvate, 100 U/ml penicillin, and 100 µg/ml streptomycin, pH 7.2).

Oocytes were injected using a Nanoject II injector (Drummond Scientific Company, Philadelphia, PA) with 30-50nL of RNA loaded into pulled 3.5" micropipettes (Drummond Scientific Company, Philadelphia, PA). Injected oocytes were resuspended in ND98 Culture solution and left covered for 2-3d.

Two-Microelectrode Voltage Clamp (TEVC) Recordings

After developing for 2-3 days, the injected oocytes were measured for membrane current in a two-microelectrode voltage clamp (TEVC) system. Preparations, techniques, and analyses of electrophysiology data were adapted from Clancy et al., 2009. Borosilicate glass microelectrodes were filled with 3M KCl solution, while pellet electrodes were suspended in a 1mM NaCl bath and isolated using an agarose bridge. Oocytes were placed in a bath with ND98 recording solution (98mM NaOH, 2mM KCl, 1mM $CaCl_2$, 5mM HEPES, pH 7.2) perfusing at 0.5-2 mL/min and recorded at room temperature (20ºC – 22ºC).

A CA-1B amplifier (Dagan Instruments, Minneapolis, MN) and the Digitdata 1440A/pClamp 10 acquisition system was used to collect data, which were low-pass filtered at 5kHz and digitized between 4 and 10 kHz. Clampfit (Molecular Devices) was used to record the raw data denoting current at each voltage (IV). Voltage-activation (GV) data was fitted with a single Boltzmann curve with the equation $G(V) = [(I_V – A_1) / (A_2 – A_1)$, where G(V) denotes the conductance at a given voltage V, I_V is the current at a given voltage V, A_1 is the minimum, and A_2 is the maximum. The data was fitted to this curve using OriginLab (Northampton, MA) software.

To measure the time course of channel activation, eggs were exposed to a series of 2-second depolarizing voltages beginning at -100mV and increasing to +80mV in 10mV increments. After each step, eggs were held at repolarizing potential of –40mV for 0.5 seconds, then –100mV for 10 seconds.

Eggs expressing the D2-23 + S349 split mutations underwent additional electrophysiology testing to verify their rapid inactivation of current. The eggs were exposed to a series of back-to-back depolarizing steps. Between these depolarizing steps, the egg was exposed to a repolarizing voltage for a variable amount of time. This gap began at 0.51s and increased to 0.65s over 8 sweeps, increasing roughly 0.02s each step.

Confocal Microscope Visualization

After processing for 2-3 days, *Xenopus laevis* oocytes injected with GFP-tagged hElk1 underwent visualization in a confocal microscope system (Zeiss, Thornwood, NY). A plastic petri dish with a small hole cut out in the middle was placed over top of the coverslip of the microscope to hold the injected eggs. Microscopy techniques were performed as done by Hertzler et al., 2023. These experiments utilized an LSM800 inverted confocal microscope that was on an Axio Observer Z1 stand. This microscope was equipped with a Zeiss Plan-APOCHROMAT 63x DIC objective and GaAsP detectors. Images were recorded using an AxioCam 506 mono camera and imaged using a Zeiss Axio Imager.M2 widefield system. Cross-sectional images were taken of injected eggs at 63x magnification to visualize the presence of both WT and mutant hElk1 channels on the cell membrane.

Chapter 3: Results

The Effects of D2-136 and S349 Split Mutations On hElk1 Current Conductivity

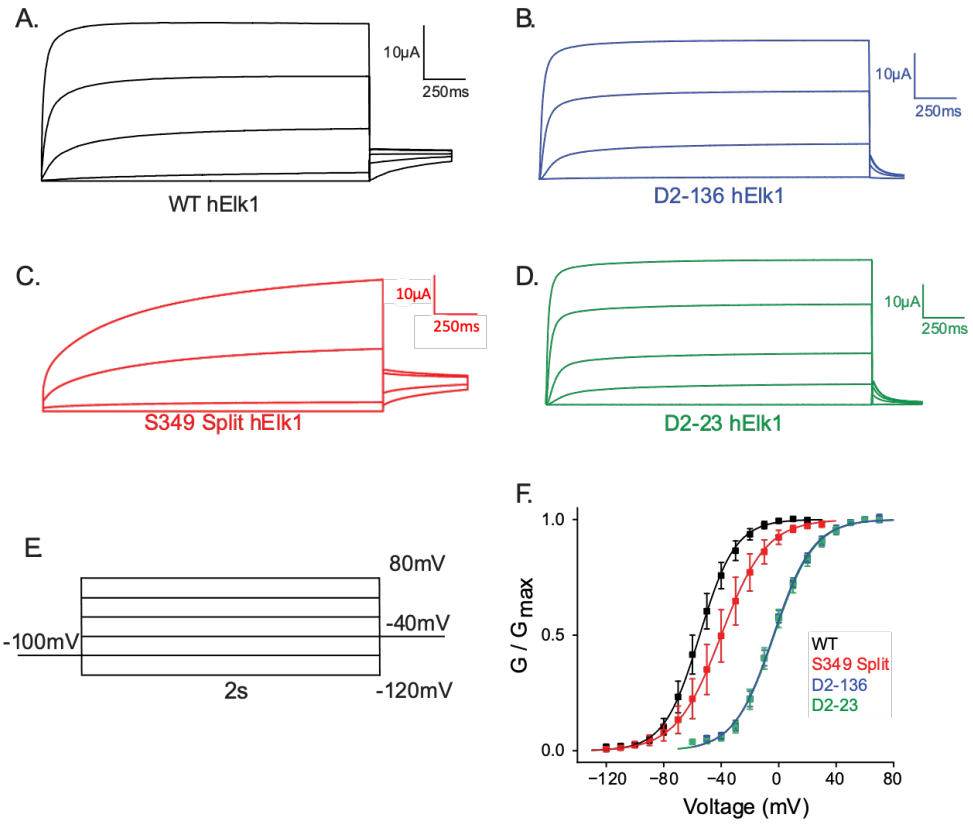

Figure 3: Potassium Current Traces of Mutant hElk1 Channels.

Example potassium current traces of (A) Wild type hElk1 (n=15, V_{50} = -54.93mV), (B) hElk1 with the PAS domain removed (n=8, V_{50} = -3.61mV) (C) hElk1 with a separated voltage sensor and pore (n= 12, V_{50} = -39.96mV), and hElk1 with the PAS-cap removed (n=9, V_{50} = -3.13mV). All currents were recorded using the voltage clamp protocol in (E), which issued 10mV steps of voltage from –120mV to 80mV with a holding potential of –100mV and a post-step potential of –40mV. (E) A comparison of the GV curves of the four mutant channels at different voltages.

Given the fact that severing the S4-S5 linker in other EAG superfamily channels shifts their conductance, we were interested in how this mutation would present itself in hElk1 channels (Tomczak et al., 2017) (Lorinczi et al., 2015). As seen in Figure 3A, wild type hElk1 channels reach their peak current relatively rapidly. This current is maintained through the remainder of the voltage step, showing the characteristic lack of inactivation in these channels. The current trace of the S349 split hElk1 mutant, on the other hand, shows that this channel takes a longer time to reach its peak current compared to the wild type, as seen in Figure 3C. The current trace for D2-136 hElk1 can be seen in Figure 3B, which reaches its peak current relatively quickly and is thus more similar to WT hElk1 than S349 Split hElk1 in terms of current kinetics. The current trace of D2-23 hElk1 in Figure 3D is nearly identical to that of WT hElk1 and D2-136 hElk1.

The GV curve displayed in Figure 3E gives a normalized comparison of the conductivities of WT hElk1, S349 split hElk1, D2-136 hElk1, and D2-23 hElk1 at varying voltages. These channels all exhibit a sigmoidal relationship between voltage and conductance. The conductivities of these channels were derived by normalizing their current at each voltage, thus indicating the proportion of their maximum current they were producing during each step of the protocol. Normalized conductance values range from 0 to 1, with 0 indicating channels are closed, and 1 indicating channels are fully open. The midpoint of the GV curve of a channel, known as the half-activation voltage (V_{50}), is the point at which channels are allowing exactly 50% of their maximum current. It is also represents the threshold at which channels are colloquially said to "activate." The V_{50} of the WT hElk1 control was measured to be -54.93mV, which is consistent with prior studies (Li et al., 2015). However, the V_{50} of the S349 split hElk1 channel was right-shifted to a value of -39.96mV. The D2-136 hElk1 and D2-23 hElk1 mutants experienced much more profound right shifts, with V_{50} values of -3.61mV and –3.13mV, respectively. This data matches previous GV characterization of D2-136 hElk1 (Li et al., 2015).

D2-23 + S349 Split hElk1 Recovers Small, Transient Current in hElk1

Since combining the D2-136 and S349 split mutations eliminated all functionality of the channel, we were interested in how combinatorial mutations would affect hElk1, specifically the D2-23 and S349 split mutations As seen in Figure 4C, D2-23 + S349 split hElk1 showed a transient current trace that lasted only milliseconds. This current reached its peak of peak of ~1μA rapidly, then almost immediately disappeared in a manner of inactivation. This current is much different than D2-23 hElk1 that is not split between VSD and PD, which shows no inactivation and produces a current similar in size to WT, S349 Split, and D2-136 hElk1. It also exhibits a right-shifted GV curve with a V_{50} value of –3.13, nearly identical to D2-136 hElk1 (Figure 3D).

Because of the small magnitude and transient nature of this current, we wanted to ensure that this was current produced by the channel, rather than native current from the egg or a problem with the electrophysiology apparatus. As negative controls, we measured the current produced in uninjected eggs and tested D2-23 + S349 split hElk1-injected eggs of multiple independent sample groups. When we exposed uninjected eggs to the voltage protocol in Figure 4A that we had used for testing, there was no current. Furthermore, D2-23 + S349 split hElk1 eggs from different injection groups spanning multiple months all showed the same transient current.

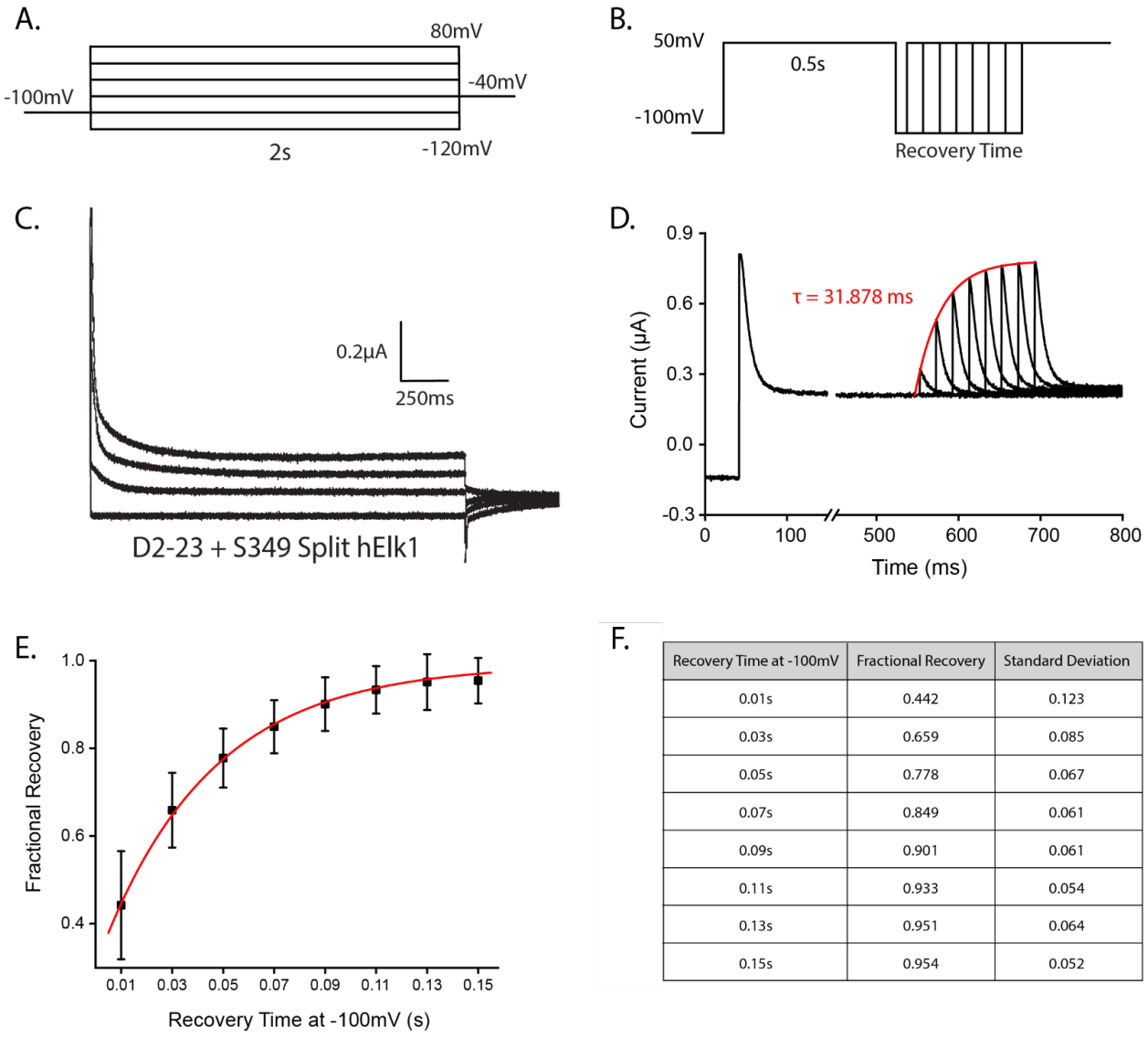

Recovery Time at -100mV	Fractional Recovery	Standard Deviation
0.01s	0.442	0.123
0.03s	0.659	0.085
0.05s	0.778	0.067
0.07s	0.849	0.061
0.09s	0.901	0.061
0.11s	0.933	0.054
0.13s	0.951	0.064
0.15s	0.954	0.052

Figure 4: Potassium Current Traces of D2-23 + S349 split hElk1

(A) Voltage clamp protocol issuing 10mV steps of voltage from –120mV to 80mV with a holding potential of –100mV and a post-step potential of –40mV. (B) Example current produced by D2-23 + S349 split hElk1 channels using the protocol in A. (C) Double pulse protocol for examining the inactivation of D2-23 S349 split hElk1 channels. This is comprised of a standard 0.5s initial depolarizing pulse at 50mV, then a variable-length hyperpolarizing 'recovery time' pulse before the second depolarizing pulse. (D)

Example current produced by D2-23 + S349 Split hElk1 channels using the protocol in B. The red line represents an exponential decay curve fitted to the peak current of each pulse, where τ = 31.878 ms. (E) Exponential decay curve of fractional recovery in D2-23 + S349 Split hElk1, where $\tau = 43.315 \pm 13.379$ms. Fractional recovery was measured as the peak current during the second 50mV depolarizing pulse divided by the peak current during the first 50mV depolarizing pulse. Recovery time is represented as the length of the hyperpolarizing –100mV pulse that occurred before the second depolarizing 50mV pulse. (F) Table depicting the fractional recovery values of D2-23 + S349 Split hElk1 at each recovery time, as well as the standard deviation for each fractional recovery value. Data was recorded from n=13 oocytes.

In addition to the standard 2-second depolarizing voltage steps that we used to collect GV and current data from WT, S349, D2-23, D2-136, and D2-136 + S349 split hElk, we also subjected the D2-23 + S349 split mutant to a 'double pulse' protocol. This double pulse experiment issued a sequence of two depolarizing steps of 50mV with a hyperpolarizing period of –100mV in between the steps. The length of the hyperpolarizing step increased with each sweep, beginning at 0.01s on the first sweep and reaching 0.15s by the eighth sweep (Figure 4B). As seen in Figure 4D of an example trace for D2-23 + S349 Split hElk1, the channels produced a similar peak current (0.5-1μA) during the first depolarizing step in all eight sweeps. However, as the recovery time increased, so did the peak current that the channels produced during the second depolarizing step. To normalize these values between samples, fractional recovery was measured, which represents the peak current of the second sweep as a fraction of the peak current of the first sweep. As shown in Figures 4D and 4E, the fractional recovery of the mutant increased in a pattern of exponential decay as the recovery time at –100mV increased. This decay curve exhibited a time constant of 43.315 ms with a standard deviation of 13.379, shown by the red line in Figure 4D.

The D2-136 + S349 Split Mutation Affects Gating but not Trafficking in hElk1

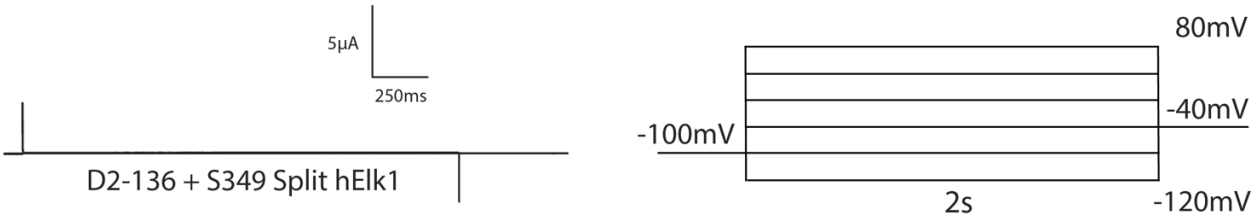

Figure 5: Sample Trace of D2-136 + S349 split hElk1 with recording protocol (n=9)

Because of the phenotype of the D2-23 + S349 split mutant, as well as the effects that the D2-136 and S349 split mutations had independently on the conductivity of hElk1, we were interested in how the channel would perform with both mutations. As seen in Figure 5, when the D2-136 and S349 split mutations were combined in hElk1, there was no current produced at any voltage. This phenotype is different than the current of D2-23 + S349 split hElk1, the other split truncated channel we tested, which showed a pattern of rapid deactivation and a peak current of roughly 1μA (Figure 4C).

We were interested in determining the cause of the lack this current. Due to the involvement of both the PAS domain and the linker in gating, we initially hypothesized that the combination of these mutations likely inhibited the gating of the channel. However, the absence of current could also occur if the channel was incapable of assembling and trafficking to the membrane. These hypotheses were influenced by prior studies in hErg channels, which found that mutations in the PAS domain altered both its gating stability and trafficking to the membrane (Ke et al., 2013). Thus, we were interested in determining which of these competing hypotheses were accurate. To test this, the C-terminal end of D2-136 + S349 split hElk1 channels were tagged with Green Fluorescent Protein (GFP).

WT hElk1 expressed well on the membrane of *Xenopus laevis* oocytes, seen by the illuminated white spots in Figure 6A. Figure 6B and 6C show that D2-23 + S349 split hElk1 and D2-136 + S349 split hElk1 both have ample expression on the membrane of the oocyte. The D2-23 + S349 split hElk1 mutant showed a more speckled pattern of expression compared to D2-136 + S349 split hElk1. These groupings of expression may represent channels in vesicular transport that are in the process of being shipped to the membrane. The levels of brightness in the images are not representative of the channels' level of expression.

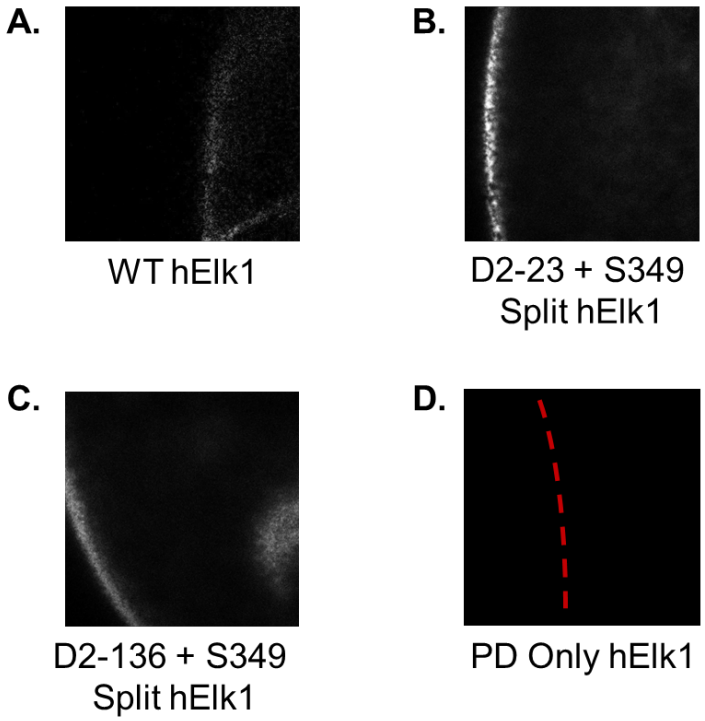

Figure 6: GFP visualization of WT and Mutant hElk1

Expression of GFP-tagged (A) WT hElk1, (B) D2-23 + S349 split hElk1, (C) D2-136 + Split hElk1, and (D) PD-only hElk1 visualized on the membrane of *Xenopus laevis* oocytes from an inverted confocal microscope. Images were visualized using a Zeiss Plan-APOCHROMAT 63x DIC objective and

processed in black and white. The white (A, B, C) and dashed red (D) arcs represent the edge of the oocyte.

Recombinant PAS Domain does not Recover Gating in D2-136 + S349 Split hElk1

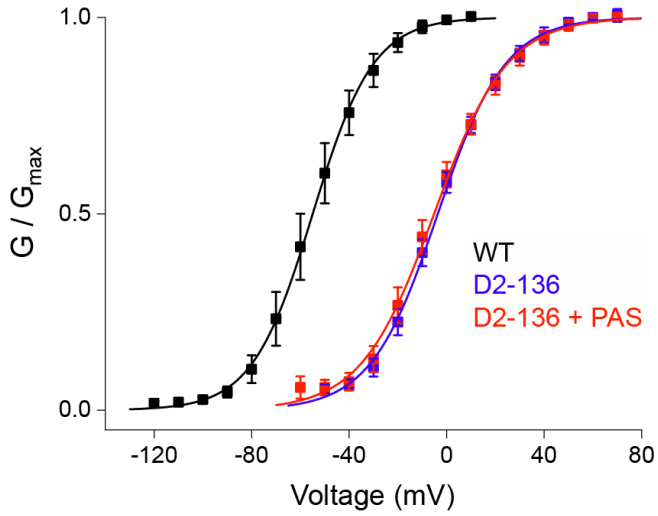

Figure 7: The effect of recombinant PAS on D2-136 hElk1

GV curves of WT hElk1 (n=15, V_{50} = -54.93mV) and D2-136 + S349 Split hElk1 with (n=7, V_{50}= -5.13mV) and without (n=8, V_{50} = -3.61mV) recombinant PAS added. The addition of the recombinant PAS domain did not recover the right shifted GV in D2-136 hElk1.

Previous studies have shown that adding recombinant PAS domain to Erg channels lacking the PAS domain recovered the deactivation gating mechanics of the channel (Gustina & Trudeau, 2009) (Wang et al., 2000). Given the close relationship between hElk1 and hErg, we were interested in whether

D2-136 hElk1 and D2-136 + S349 split hElk1 could experience a similar recovery in current production and conductivity. Recombinant PAS domains were injected with both mutant channels into oocytes and the oocytes were subjected to the voltage step protocol shown in Figure 3D. As shown above in Figure 7, the GV curves of these two channels are almost nearly identical, showing there is no little to no difference in conductivity of D2-136 + S349 split hElk1 when recombinant PAS is added. Furthermore, the V_{50} values of D2-136 hElk1 with and without recombinant PAS added were very close, measured at –3.61mV and –5.13mV, respectively.

Chapter 4: Discussion

The broad functions and applications of hElk channels, the destructive effects of their deletion in mouse models, and the uncertainty of their gating mechanics and inter-subunit relationships make them an extremely interesting protein for investigation (Hermanstyne et al., 2023) (Zhang et al., 2010). To further elucidate how these channels function, we performed many experiments branching off the key findings made by various studies from other laboratories and our own. Specifically, we used electrophysiological and fluorescent visualization techniques to assess the relationship between different domains within hElk1 subunits and how they may interact with one another to regulate gating.

Prior studies found that the S4-S5 linker played a different role in EAG superfamily channels than in many other families of Kv channels. This is hypothesized to be the result of the EAG channels lacking a domain swapped architecture, which prevents the S4-S5 linker from interacting directly with the bottom of the S6 domain and pore of the channel (Lorinczi et al., 2015) (Tomczak et al., 2017). These studies showed that the severance of the S4-S5 linker does not eliminate the channel gating. Our findings for an Elk subfamily channel were consistent with this data, as shown in Figure 3C. The S349 split hElk1 still produced a strong current similar in magnitude to WT hElk1, indicating that the S4-S5 linker is not required for voltage-gating in hElk1. However, S349 Split hElk1 exhibited a slower activation than WT hElk1, as it took longer to reach its peak current at a given voltage step. Furthermore, its right shifted V_{50} value indicates that the channel required more depolarized voltages to conduct a similar level of current as WT hElk1. These findings suggest that the S4-S5 linker physically connecting the VSD and PD is essential for stabilizing the open state of the channel.

D2-136 hElk1 experienced a more profound right shifted V_{50} value than S349 split hElk1, while also reaching its peak current much quicker (Li et al., 2015). Thus, within a given voltage step, D2-136 hElk1 could open relatively quickly, but it was only able to activate at extremely depolarized voltages (Figure 3B). We observed a similar phenotype in D2-23 hElk1, where only the cap of the PAS domain

was removed. The right shifted GV of both channels represents their instability in the open state. These findings suggest that the residues in the PAS-cap may play a role in the transduction of the voltage detection in the channel and its stabilization in the open state; with its removal in the D2-23 mutant, channels were still closed at the same voltage where WT hElk1 was conducting 76% of its peak current. However, this phenotype did not change when the rest of the PAS domain past residue 23 was removed in the D2-136 mutant.

These findings led us to investigate how introducing a split in the S4-S5 Linker to D2-23 hElk1 would alter the channel gating. The PAS-cap is critical for stabilizing the open state of hElk1 through a hypothesized interaction with the membrane phospholipid phosphatidylinositol bisphosphate (PIP_2) (Li et al., 2015). Thus, if the PAS domain and S4-S5 linker were involved in the gating of the channel, we would expect the D2-23 + S349 Split hElk1 to display some current but ultimately experience rapid destabilization in the open state, mimicking the kinetics of inactivation. This is because the presence of and critical residues in the rest of the PAS domain (24-136) would likely stabilize the channel enough for it to open, but the lack of a PAS-cap would cause rapid open-state destabilization (Li et al., 2014) (Gustina & Trudeau, 2011).

When subjected to the voltage step protocol, D2-23 + S349 split hElk1 expressed a small transient current that disappeared almost immediately (Figure 4C). These kinetics indicated that the VSD could transduce its conformational change to the PD and allow it to open, but the channel was not stable enough to maintain this state and would thus inactivate. The small magnitude of current may have been caused by the expression of fewer channels expressed in the membrane. However, given the ample presence of D2-23 + S349 Split hElk1 on oocyte membranes, this weak current is likely due to rapid inactivation overtaking the activation rate of the channels (Figure 6B). To further investigate this inactivation, we used the ‘double pulse protocol’ in Figure 4B to test the rate of recovery from inactivation. The channels were subjected to a depolarizing voltage and then given a hyperpolarizing pulse of variable time, also known as the recovery time, before receiving a second depolarizing voltage. This hyperpolarizing pulse would allow

the D2-23 + S349 split hElk1 channels that inactivated during the first depolarizing step to change their conformation to the deactivated state and thus reopen during the second depolarizing pulse. We hypothesized that the peak current during the second depolarizing pulse would increase as the recovery time increased. This is because a longer recovery time would allow more channels to achieve their deactivated conformation. This means a greater proportion of channels could reopen during the second depolarization and thus conduct a greater total current. The peak currents at each sweep fit this trend in our experiment. The current produced during the second depolarizing pulse increased in a manner of exponential decay as the recovery time increased, be seen by the curve in red in Figure 4E, as well as the fractional recovery values in Figure 4F.

Conversely, we expected that the absence of the entire PAS domain and a split S4-S5 linker in D2-136 + S349 split hElk1 would show no current because its extreme instability in the open state would render it in a persistently closed-inactivated state. Consistent with our predictions, D2-136 S349 split hElk1 channels expressed no current at any voltage (Figure 5). This loss of function could be caused by an issue in hElk1's gating process or its assembly and trafficking to the membrane. Our previous results demonstrated that the PAS domain and S4-S5 linker are both implicated in stabilizing the gating process of the channel. However, studies also found that mutations in the PAS domain of Erg channels cause a significant decrease in protein stability that ultimately led to deficiencies in trafficking (Gayen et al., 2011) (Ke et al., 2013). These competing results raised the question of whether the VSD and PD in D2-136 + S349 Split hElk1 co-assemble but do not gate, or simply do not co-assemble.

Using our GFP tagged D2-136 + S349 hElk1, we verified that the lack of current seen in the electrophysiology data of this channel was due to changes in gating and not in trafficking to the membrane. The GFP-tagged PD of hElk1 was injected without any hElk1 VSD to serve as a negative control for this experiment. As shown in Figure 6D, the PD could not reach the membrane by itself, suggesting that it may be degraded within the endoplasmic reticulum or that it is not being tagged for transport. However, the PD was present on the membrane with any given VSD, whether it was WT VSD,

D2-136 VSD, or D2-23 VSD (Figure 6A, 6B, 6C). The more speckled pattern of D2-23 + S349 Split hElk1 may represent channels in vesicular transport to the membrane (Figure 6B). Ultimately, these findings demonstrate that both the VSD and PD are needed for hElk1 to reach the membrane, but that its construction and trafficking do not specifically require a PAS domain or an intact S4-S5 linker.

The difference in current traces of D2-23 + S349 split hElk1 and D2-136 + S349 split hElk1 suggest that different regions within the PAS domain may have specific roles in the gating process. Two areas of interest include R57, as well as residues 88 – 94. R57 has been shown to form a salt bridge with a residue of the CNBHD domain, and that this connection is absent when the R57 residue is mutated (Dai & Zagotta, 2017) (Li et al., 2014). Conversely, residues 88 – 94 have been shown to have high affinity for the S4-S5 linker peptide (Li et al., 2010). Despite the presence of these residues in D2-23 hElk and their absence in D2-136 hElk1, both channels showed the same GV curve and current kinetics likely because the intact S4-S5 linker sufficiently stabilized the channels (Figure 3B & 3D). Conversely, the lack of these residues combined with a severed S4-S5 linker in D2-136 + S349 split hElk1 may have led to the instability in the channel that prevented it from producing current (Figure 5). The presence and interaction of the R56 residue and CNBHD domain in D2-23 + S349up hElk1 may have provided enough stabilization for this channel to open enough to produce a small transient current (Figure 4C). Although residues 88-94 were also present in this mutant, their interaction with the S4-S5 linker may have been compromised due to the split in the linker. Without this additional interaction providing more open state stability to the channel, this could be why the channel immediately closed after opening. If this were the case, then it would indicate that the PAS-CNBHD interaction may assist in the opening and closing of the channel, whereas interactions with the linker may be geared toward open-state stabilization (Li et al., 2015).

We also found that adding recombinant PAS domain to D2-136 + S349 split hElk1 did not assist in recovering any aspect of the channel current. This result was unexpected because the phenotype of Erg channels lacking the PAS domain was shown to recover and mimic the WT phenotype when recombinant

PAS was added (Gustina & Trudeau, 2009) (Wang et al., 2000). These studies primarily focused on the recovery of slow deactivation, which is characteristic to Erg channel current. But, as a common delayed rectifier, hElk1 does not experience this deactivation, which can be seen in Figure 3A of a sample trace of WT hElk1. Once the current reaches its peak, its magnitude is maintained, whereas in Erg channels, it would slowly dissipate. If recombinant PAS can reverse rapid deactivation in Erg channels, yet it has been thoroughly demonstrated that it is still essential to hElk1 gating, it may be the case that it needs to be positioned specifically to regulate hElk1 channel gating. This positioning may be assisted by its direct attachment to the channel, so that intermolecular interactions with the S4-S5 linker are facilitated.

Ultimately, this research was able to expand on the interplay between the PAS domain and S4-S5 linker in the gating of hElk1 channels. Through electrophysiology data and fluorescence imaging, we found that the S4-S5 linker and PAS domain together play a critical role in hElk1 gating. The presence of at least one of the two structures is enough to functionally connect the VSD and PD, albeit with a delay in voltage-dependent activation. However, when both regions are absent from the channel, hElk1 is unable to conduct any current, but it is still capable of assembling and trafficking to the membrane. Thus, this lack of current is likely because the absence of a PAS domain and intact S4-S5 linker has an additive effect on the destabilization of the channel, forcing it into a persistently closed-inactivated state. The interplay between the PAS domain and PIP_2 could be a potential avenue for future endeavors investigating how split truncated hElk1 channels interact with surrounding membrane phospholipids. Prior research has found that PIP_2 interacts with the PAS-cap to influence open state stabilization (Li et al., 2015). Expressing S349 split hElk1 in the absence of PIP_2 in the membrane may show the same inactivating phenotype in D2-23 + S349 split hElk1, as the PAS-cap would not be able to stabilize the channel via PIP_2.

Appendix A

Primer Sequences

S349 Split hElk1	
Forward VSD	TCCTAGCTAGCCCCCATGCCGGTTATGAAAGGATTACTGG
Reverse VSD	GAAGCCTCGAGTCAGGAATAGCGGTCTAACTTCTG
Forward PD	TCCTAGCTAGCCACCATGCAACACAGTACTATCGTCCTG
Reverse PD	GAAGCCTCGAGTCATACATTTATGGCTTTGT
D2-136 hElk1	
Forward	TCCTAGCTAGCCCCCATGGTGAAGATTACTCCAGAAG
Reverse	GAAGCCTCGAGTCATACATTTATGGCTTTGT
D2-23 hElk1	
Forward	TCCTAGCTAGCCCACCATGACACATAGCAACTTCATCCTT
Reverse	GAAGCCTCGAGTCATACATTTATGGCTTTGT
D2-136 + S349 Split hElk1	
Forward	TCCTAGCTAGCCCCCATGGTGAAGATTACTCCAGAAG
Reverse	GAAGCCTCGAGTCAGGAATAGCGGTCTAACTTCTG
D2-23 + S349 Split hElk1	
Forward	GCATCAATTAACCCTCACTAAAGGCCAC
Reverse	TATCTAGCGCGTAATACGACTCACTAT
Recombinant Pas Domain	
Forward PAS domain	CCATGATTACGCCAAGCGCGC
Reverse PAS domain	ACTTCTAGAGGGCACTAATATCATGTATCTGTTATATCTTTGAAC
Forward UTR region	TTTCCGGAGTATAAAGTTTCTTGATATTAGTGCCCTCTAGAAGT
Reverse UTR region	GCGCGTAATACGACTCACTATAG
hElk1 PD + GFP	
Forward PD	TCCTAGCTAGCCACCATGCAACACAGTACTATCGTCCTG
Reverse PD	TGAGCCGCCTGAGCCGCCTACATTTAT
Forward GFP	GGCGGCTCAGGCGGCTCAATGGTGAG
Reverse GFP	GCATAGAATTCCTTGTACAGCTCGTCC

BIBLIOGRAPHY

Clancy, S. M., Chen, B., Bertaso, F., Mamet, J., & Jegla, T. (2009). Kcne1 and kcne3 β-subunits regulate membrane surface expression of kv12. 2 k+ channels in vitro and form a tripartite complex in vivo. *PLoS ONE*, *4*(7), e6330. https://doi.org/10.1371/journal.pone.0006330

Cabral, J. H. M., Lee, A., Cohen, S. L., Chait, B. T., Li, M., & Mackinnon, R. (1998). Crystal Structure and Functional Analysis of the HERG Potassium Channel N Terminus: A Eukaryotic PAS Domain. *Cell*, *95*(5), 649–655. https://doi.org/10.1016/S0092-8674(00)81635-9

Codding, S. J., Johnson, A. A., & Trudeau, M. C. (n.d.). Gating and regulation of KCNH (ERG, EAG, and ELK) channels by intracellular domains. *Channels*, *14*(1), 294–309. https://doi.org/10.1080/19336950.2020.1816107

Curran, M. E., Splawski, I., Timothy, K. W., Vincent, G. M., Green, E. D., & Keating, M. T. (1995). A molecular basis for cardiac arrhythmia: HERG mutations cause long QT syndrome. *Cell*, *80*(5), 795–803. https://doi.org/10.1016/0092-8674(95)90358-5

Dai, G., & Zagotta, W. N. (n.d.). Molecular mechanism of voltage-dependent potentiation of KCNH potassium channels. *ELife*, *6*, e26355. https://doi.org/10.7554/eLife.26355

de la Peña, P., Domínguez, P., & Barros, F. (2018). Gating mechanism of Kv11.1 (hERG) K+ channels without covalent connection between voltage sensor and pore domains. *Pflügers Archiv - European Journal of Physiology*, *470*(3), 517–536. https://doi.org/10.1007/s00424-017-2093-9

Durell, S. R., & Guy, H. R. (1992). Atomic scale structure and functional models of voltage-gated potassium channels. *Biophysical Journal*, *62*(1), 238–247; discussion 247-250. https://doi.org/10.1016/S0006-3495(92)81809-X

Engeland, B., Neu, A., Ludwig, J., Roeper, J., & Pongs, O. (1998). Cloning and functional expression of rat ether-à-go-go-like K+ channel genes. *The Journal of Physiology*, *513*(Pt 3), 647–654. https://doi.org/10.1111/j.1469-7793.1998.647ba.x

Gayen, S., Li, Q., Chen, A. S., Nguyen, T. H. T., Huang, Q., Hill, J., & Kang, C. (2011). An NMR study of the N-terminal domain of wild-type hERG and a T65P trafficking deficient hERG mutant. *Proteins: Structure, Function, and Bioinformatics*, *79*(8), 2557–2565. https://doi.org/10.1002/prot.23089

Gustina, A. S., & Trudeau, M. C. (2009). A recombinant N-terminal domain fully restores deactivation gating in N-truncated and long QT syndrome mutant hERG potassium channels. *Proceedings of the National Academy of Sciences*, *106*(31), 13082–13087. https://doi.org/10.1073/pnas.0900180106

Gustina, A. S., & Trudeau, M. C. (2012). HERG potassium channel regulation by the N-terminal eag domain. *Cellular Signalling*, *24*(8), 1592–1598. https://doi.org/10.1016/j.cellsig.2012.04.004

Haitin, Y., Carlson, A. E., & Zagotta, W. N. (2013). The structural mechanism of KCNH-channel regulation by the eag domain. *Nature*, *501*(7467), Art. 7467. https://doi.org/10.1038/nature12487

Hermanstyne, T. O., Yang, N.-D., Granados-Fuentes, D., Li, X., Mellor, R. L., Jegla, T., Herzog, E. D., & Nerbonne, J. M. (2023). Kv12-encoded K+ channels drive the day–night switch in the repetitive firing rates of SCN neurons. *Journal of General Physiology*, *155*(9), e202213310. https://doi.org/10.1085/jgp.202213310

Hertzler, J. I., Bernard, A. R., & Rolls, M. M. (2023). Dendrite regeneration mediates functional recovery after complete dendrite removal. *Developmental Biology*, *497*, 18–25. https://doi.org/10.1016/j.ydbio.2023.03.001

Jensen, M. Ø., Jogini, V., Borhani, D. W., Leffler, A. E., Dror, R. 0., & Shaw, D. E. (2012). Mechanism of Voltage Gating in Potassium Channels. *Science*, *336*(6078), 229–233.

Jogini, V., & Roux, B. (2007). Dynamics of the Kv1.2 Voltage-Gated K+ Channel in a Membrane Environment. *Biophysical Journal*, *93*(9), 3070–3082. https://doi.org/10.1529/biophysj.107.112540

Jones, E. M. C., Roti Roti, E. C., Wang, J., Delfosse, S. A., & Robertson, G. A. (2004). Cardiac IKr Channels Minimally Comprise hERG 1a and 1b Subunits*. *Journal of Biological Chemistry*, *279*(43), 44690–44694. https://doi.org/10.1074/jbc.M408344200

Kandel, E., Schwartz, J., Jessell, T., Siegelbaum, S., & Hudspeth, A. (2013). *Principles of neural science* (Fifth Edition). McGraw Hill.

Kazmierczak, M., Zhang, X., Chen, B., Mulkey, D. K., Shi, Y., Wagner, P. G., Pivaroff-Ward, K., Sassic, J. K., Bayliss, D. A., & Jegla, T. (2013). External pH modulates EAG superfamily K+ channels through EAG-specific acidic residues in the voltage sensor. *Journal of General Physiology*, *141*(6), 721–735. https://doi.org/10.1085/jgp.201210938

Ke, Y., Ng, C. A., Hunter, M. J., Mann, S. A., Heide, J., Hill, A. P., & Vandenberg, J. I. (2013). Trafficking defects in PAS domain mutant Kv11.1 channels: Roles of reduced domain stability and altered domain–domain interactions. *Biochemical Journal*, *454*(1), 69–77. https://doi.org/10.1042/BJ20130328

Labro, A. J., Raes, A. L., Grottesi, A., Van Hoorick, D., Sansom, M. S. P., & Snyders, D. J. (2008). Kv Channel Gating Requires a Compatible S4-S5 Linker and Bottom Part of S6, Constrained by Non-interacting Residues. *Journal of General Physiology*, *132*(6), 667–680. https://doi.org/10.1085/jgp.200810048

Li, Q., Gayen, S., Chen, A. S., Huang, Q., Raida, M., & Kang, C. (2010). NMR solution structure of the N-terminal domain of hERG and its interaction with the S4–S5 linker. *Biochemical and Biophysical Research Communications*, *403*(1), 126–132. https://doi.org/10.1016/j.bbrc.2010.10.132

Li, Q., Ng, H. Q., Yoon, H. S., & Kang, C. (2014). Insight into the molecular interaction between the cyclic nucleotide-binding homology domain and the eag domain of the hERG channel. *FEBS Letters*, *588*(17), 2782–2788. https://doi.org/10.1016/j.febslet.2014.05.056

Li, X., Anishkin, A., Liu, H., van Rossum, D. B., Chintapalli, S. V., Sassic, J. K., Gallegos, D., Pivaroff-Ward, K., & Jegla, T. (2015). Bimodal regulation of an Elk subfamily K+ channel by phosphatidylinositol 4,5-bisphosphate. *Journal of General Physiology*, *146*(5), 357–374. https://doi.org/10.1085/jgp.201511491

Long, S. B., Campbell, E. B., & Mackinnon, R. (2005). Voltage sensor of Kv1.2: Structural basis of electromechanical coupling. *Science (New York, N.Y.)*, *309*(5736), 903–908. https://doi.org/10.1126/science.1116270

Lörinczi, É., Gómez-Posada, J. C., de la Peña, P., Tomczak, A. P., Fernández-Trillo, J., Leipscher, U., Stühmer, W., Barros, F., & Pardo, L. A. (2015). Voltage-dependent gating of KCNH potassium channels lacking a covalent link between voltage-sensing and pore domains. *Nature Communications*, *6*(1), Art. 1. https://doi.org/10.1038/ncomms7672

Mitcheson, J. S., Chen, J., Lin, M., Culberson, C., & Sanguinetti, M. C. (2000). A structural basis for drug-induced long QT syndrome. *Proceedings of the National Academy of Sciences*, *97*(22), 12329–12333. https://doi.org/10.1073/pnas.210244497

Mortensen, L. S., Schmidt, H., Farsi, Z., Barrantes-Freer, A., Rubio, M. E., Ufartes, R., Eilers, J., Sakaba, T., Stühmer, W., & Pardo, L. A. (2015). KV 10.1 opposes activity-dependent increase in Ca^{2+} influx into the presynaptic terminal of the parallel fibre-Purkinje cell synapse. *The Journal of Physiology*, *593*(1), 181–196. https://doi.org/10.1113/jphysiol.2014.281600

Pisupati, A., Mickolajczyk, K. J., Horton, W., van Rossum, D. B., Anishkin, A., Chintapalli, S. V., Li, X., Chu-Luo, J., Busey, G., Hancock, W. O., & Jegla, T. (2018). The S6 gate in regulatory Kv6 subunits restricts heteromeric K+ channel stoichiometry. *Journal of General Physiology*, *150*(12), 1702–1721. https://doi.org/10.1085/jgp.201812121

Robertson, G. A., Warmke, J. M., & Ganetzky, B. (1996). Potassium currents expressed from Drosophila and mouse eag cDNAs in Xenopus oocytes. *Neuropharmacology*, *35*(7), 841–850. https://doi.org/10.1016/0028-3908(96)00113-x

Ruta, V., Chen, J., & MacKinnon, R. (2005). Calibrated Measurement of Gating-Charge Arginine Displacement in the KvAP Voltage-Dependent K+ Channel. *Cell*, *123*(3), 463–475. https://doi.org/10.1016/j.cell.2005.08.041

Saganich, M. J., de Miera, E. V.-S., Nadal, M. S., Baker, H., Coetzee, W. A., & Rudy, B. (1999). Cloning of Components of a Novel Subthreshold-Activating K+ Channel with a Unique Pattern of Expression in the Cerebral Cortex. *The Journal of Neuroscience*, *19*(24), 10789–10802. https://doi.org/10.1523/JNEUROSCI.19-24-10789.1999

Tomczak, A. P., Fernández-Trillo, J., Bharill, S., Papp, F., Panyi, G., Stühmer, W., Isacoff, E. Y., & Pardo, L. A. (2017). A new mechanism of voltage-dependent gating exposed by KV10.1 channels interrupted between voltage sensor and pore. *Journal of General Physiology*, *149*(5), 577–593. https://doi.org/10.1085/jgp.201611742

Trudeau, M. C., Warmke, J. W., Ganetzky, B., & Robertson, G. A. (1995). HERG, a human inward rectifier in the voltage-gated potassium channel family. *Science (New York, N.Y.)*, *269*(5220), 92–95. https://doi.org/10.1126/science.7604285

Wang, J., Myers, C. D., & Robertson, G. A. (2000). Dynamic Control of Deactivation Gating by a Soluble Amino-Terminal Domain in HERG K+ Channels. *The Journal of General Physiology*, *115*(6), 749–758.

Wang, J., Trudeau, M. C., Zappia, A. M., & Robertson, G. A. (1998). Regulation of Deactivation by an Amino Terminal Domain in Human Ether-à-go-go –related Gene Potassium Channels. *The Journal of General Physiology*, *112*(5), 637. https://doi.org/10.1085/jgp.112.5.637

Wang, W., & MacKinnon, R. (2017). Cryo-EM Structure of the Open Human Ether-à-go-go-Related K+ Channel hERG. *Cell*, *169*(3), 422-430.e10. https://doi.org/10.1016/j.cell.2017.03.048

Wang, Z.-J., Ghorbani, M., Chen, X., Tiwari, P. B., Klauda, J. B., & Brelidze, T. I. (2023). Molecular mechanism of EAG1 channel inhibition by imipramine binding to the PAS domain. *Journal of Biological Chemistry*, *299*(12). https://doi.org/10.1016/j.jbc.2023.105391

Wang, Z.-J., Soohoo, S. M., Tiwari, P. B., Piszczek, G., & Brelidze, T. I. (2020). Chlorpromazine binding to the PAS domains uncovers the effect of ligand modulation on EAG channel activity. *Journal of Biological Chemistry*, *295*(13), 4114–4123. https://doi.org/10.1074/jbc.RA119.012377

Warmke, J. W., & Ganetzky, B. (1994). A family of potassium channel genes related to eag in Drosophila and mammals. *Proceedings of the National Academy of Sciences of the United States of America*, *91*(8), 3438–3442.

Whicher, J. R., & MacKinnon, R. (2016). Structure of the voltage-gated K+ channel Eag1 reveals an alternative voltage sensing mechanism. *Science (New York, N.Y.)*, *353*(6300), 664–669. https://doi.org/10.1126/science.aaf8070

Zhang, X., Bertaso, F., Yoo, J. W., Baumgärtel, K., Clancy, S. M., Lee, V., Cienfuegos, C., Wilmot, C., Avis, J., Hunyh, T., Daguia, C., Schmedt, C., Noebels, J., & Jegla, T. (2010). Deletion of the potassium channel Kv12.2 causes hippocampal hyperexcitability and epilepsy. *Nature Neuroscience*, *13*(9), 1056–1058. https://doi.org/10.1038/nn.2610

Zhang, X., Bursulaya, B., Lee, C. C., Chen, B., Pivaroff, K., & Jegla, T. (2009). Divalent Cations Slow Activation of EAG Family K+ Channels through Direct Binding to S4. *Biophysical Journal*, *97*(1), 110–120. https://doi.org/10.1016/j.bpj.2009.04.032

Zou, A., Lin, Z., Humble, M., Creech, C. D., Wagoner, P. K., Krafte, D., Jegla, T. J., & Wickenden, A. D. (2003). Distribution and functional properties of human KCNH8 (Elk1) potassium channels. *American Journal of Physiology-Cell Physiology*, *285*(6), C1356–C1366. https://doi.org/10.1152/ajpcell.00179.2003